Accepted Manuscript

Please cite this article as: del Val, J., Comesaña, R., Riveiro, A., Lusquiños, F., Quintero, F., Boutinguiza, M., et al. (2018). Laser direct writing of co-superalloy lines for micro-fabrication applications. *Surface and Coatings Technology, 345*, 76-88. doi:10.1016/j.surfcoat.2018.03.089

Link to published version: https://doi.org/10.1016/j.surfcoat.2018.03.089

Laser direct writing of Co-superalloy lines for micro-fabrication applications

Jesús del Val[1], Rafael Comesaña[2], Antonio Riveiro[1], Fernando Lusquiños[1], Félix Quintero[1], Mohamed Boutinguiza[1], Juan Pou[1]

[1] Applied Physics Department, University of Vigo, EEI, Lagoas-Marcosende, Vigo, 36310, SPAIN.

[2] Materials Engineering, Applied Mechanics and Construction Dpt., University of Vigo, EEI, Lagoas-Marcosende, Vigo, 36310, SPAIN.

ABSTRACT.

Co-superalloy lines were deposited on stainless steel by a direct laser writing technique: laser micro-cladding by lateral powder injection.

With the aim of producing small strips as thin and narrow as possible, the mean size of the powder used was 8 μm. Using such fine particles makes conventional powder feeders useless, due to the formation of agglomerates unable to be feed. Therefore a new powder feeder, here described, was designed, constructed and tested. A processing parameters map was established, identifying the working window for laser micro-cladding.

The new power feeder and a high brightness, good beam quality fibre laser allowed producing fine lines just 14 μm wide and 7.2 μm thick. Microstructure and mechanical properties, in terms of Hardness and Elastic Modulus, were evaluated confirming that the fine strips maintain the main characteristics of the hardfacing alloy.

Potential applications include micro-part fabrication and repairing such as micro-moulds, and production of 3D parts at sub-millimetre scales.

Keywords: laser direct writing; Co alloy; micro-cladding.

1. **INTRODUCTION**

Laser direct writing has been the object of study of many research groups throughout the World for the last four decades [1, 2]. And is still today an active field of research due to its precision, relative simplicity, and high yielding rate; but also due to the attractive beauty of the idea behind this technique, that is “writing with light” [3, 4]. Laser direct writing comprises a family of different techniques used to deposit fine lines of a certain precursor material on a given substrate (including laser induced forward transfer (LIFT), Matrix-assisted pulsed-laser evaporation (MAPLE), laser chemical vapour deposition (LCVD), selective laser sintering (SLS), selective laser melting (SLM), or two-photon polimerization) [5, 6]. These techniques are certainly quite different but sharing the common fact that the source of energy is a laser beam.

The miniaturization of objects and devices is one of the manufacturing activities that has most evolved in the last 20 years and has been a driven force pushing the development of different laser and non- laser based techniques [7, 8]. One example of miniaturization is the micro moulds used for various applications such as microfluidics or microinjection [9]. Fabrication and repairing of such micro moulds requires the deposition of small amount of a certain material (usually hard and wear resistant) on a given surface [10]. Existing thin film techniques such as Chemical Vapour Deposition (CVD), sputtering in its different variants, pulsed laser deposition (PLD), Plasma-Assisted Chemical Vapour Deposition (PACVD) or Laser Chemical Vapour Deposition (LCVD) allow the deposition of thin layers of a certain material, with high quality (in terms of purity and homogeneity). Usually these techniques are carried out inside a high-vacuum reaction chamber. When the material needs to be deposited on a limited small place, some of the techniques require a mask (reducing flexibility), and if the thickness of the layer exceeds the micrometre, normally a long deposition time is required (exceeding the hour) [11, 12].

On the other hand, techniques available to produce thick coatings are rather difficult to be adapted to the micrometre range [13]. Laser cladding is one of these so called “thick coating” techniques that has been successfully modified to produce features at micrometre scale [14, 15].

Laser cladding is a well know technique in which a high power laser is used as energy source to melt the precursor coating material over the surface of a given substrate. At the same time a superficial thin part of the substrate is also molten in order to achieve a strong metallurgical bond [16]. The coating precursor material can be applied in different ways, being the blowing powder technique the most robust one. Laser cladding allows producing coatings made of single [17] or multiple layers [18]. Application of coatings produced by this technique range from increasing wear resistance [19-21], decreasing friction coefficient [22], improving corrosion resistance [23, 24], to biocompatibility enhancement [25-27]. Therefore a broad palette of materials have been applied by laser cladding: from superalloys [28, 29] to ceramic materials [30].

In order to apply laser cladding at the micrometric scale (micro-cladding) layers should have a thickness in the micrometre range (i.e.: geometrical features < 100μm). First attempts to produce such coatings used pre-placed pastes [14, 31, 32]. This technique allows producing thin layers (10 micrometre thickness range) and 100-200 micrometre wide. The technique comprises three main phases: pre-application of the paste, laser processing, and thermal treatment. The material finally obtained is not a molten strip but sintered powder.

Using the powder injection technique, fully dense materials were deposited by laser micro-cladding [33, 34]. Using co-axial laser micro-cladding the group of Prof. Nowotny obtained clad tracks of Al–Si alloys with lateral resolution well below 300 micrometres [35, 36]. Laser micro-cladding using the powder injection technique show its versatility in works such as that of Bo Yao et al. [37] in which 3D elements made of Ti6Al4V at submillimetre range, were produced. More recently the group of Prof. Beyer developed a new laser micro-cladding variety based on a filler wire coaxial to the laser beam [38]. The technique allows producing high quality layers being the limits to achieve very small sizes based on the diameter of commercial wires. Similar results were obtained using an off-axis wire configuration achieving layer widths between 700 and 800 micrometres [39].

This technique,as well as the powder injection one, allow a more effective use of the precursor material, being up to 100% in the case of the wire based one [39], in contrast to the powder bed techniques that require the use of a great amount of powder not all being reusable [40, 41]. Notwithstanding powder bed techniques already showed their potential to produce 3D metal microstructures such as cardiovascular stents [42].

In a previous work, our group was able to produce strips in the micrometre range (width: 50 μm, height: 20 μm) using the laser micro-cladding technique feeding the powder laterally to the laser beam axis [15, 43]. The present work is devoted to explore the limits of the technique on the production of small strips as thin and narrow as possible, while keeping the mechanical properties of deposited layer similar to those of the precursor material.

2. MATERIALS AND METHODS.

2.1. Materials.

In order to assess the achievement of the objectives set in this work, one of the most used powders in laser cladding was selected as precursor material: a hardfacing Co-superalloy [44]. In order to be able to achieve the smallest strip possible, a powder with mean particle size of 8 μm was used as precursor material (powder provided by (Sandvik Osprey; UK). Small quantities of this powder, randomly selected, were analysed by scanning electron microscopy (SEM) and X-ray Fluorescence (XRF) in order to evaluate the morphology and chemical composition. SEM micrograph of Fig. 1 shows a clearly spherical morphology of the powder particles used.

The substrates were slabs of stainless steel (AISI 316) of 60 mm × 60 mm x 10 mm (width, length and height).These plates were polished up to achieve a low surface average roughness of < 0.5 μm. This allows identifying the geometry of narrow lines to be deposited.

The complete substrate and precursor properties are summarized in Tables 1 and 2.

Table 1. Composition (%weight) of the substrate and the powder

	C	Cr	Si	W	Fe	Co	Ni	Mn	Mo	B
Precursor material (nominal)	0.8	29,5	0,8	8,7	1.0	Bal.	1.6	0.7	-	0.4
Precursor material (XRF)	0.7	28.1	0.9	7.9	0.9	54.2	1.4	0.5	-	-
Substrate (nominal)	0.08	18.0	1.0	-	Bal.	-	9.5	2.0	2.0	0.2

Table 2. Granulometry of precursor material

Mean particle size (μm)			Morphology	Tap density (g/cm^3)
D10	D50	D90		
3.5	8.0	16.0	Spherical	4.8

2.2. Deposition system

As commented previously, the laser cladding by pneumatic powder injection technique was applied to carry out the experiments. In order to allow more flexibility to position the powder with regard to the laser beam, the powder nozzle axis was placed non-coincident with the laser beam axis. This is known as off-axis nozzle geometry. To generate the clad track, a motorized stage moved the substrate with regard to the laser beam and the powder injection nozzle. The angle between the off-axis nozzle and the substrate can be varied by means of a manual micrometre positioning stage. The basic outline of the method is shown in Fig. 2.

All laser micro-cladding experiments were performed with a high brightness monomode SPI Yb:YAG fiber laser delivering a maximum power of 200 W. The wavelength of the laser radiation was 1075 nm. The laser beam was guided by means of a 50 μm core diameter fiber, coupled to the working station via expanding (x10 factor) and collimating optics, and finally focused exactly in the surface of the substrate through a doublet lens (focal length = of 80 mm) in order to reduce optical

aberration. The laser beam diameter value was (5 ± 0.5) mm at the output of the optical fiber, and before its expansion. Due to the fact that laser beam quality is a crucial parameter to achieve small lines, it was measured in terms of M^2 by means of a Spiricon (LBA-300PC) analyzer. The measurements showed a value of $M^2 < 1.2$, considered acceptable because a beam diameter of less than 10 μm on the focal plane was attained.

2.3. Micro-powder feeding system

The tendency of the precursor powder to form aggregates depends on the effect of the particle density (ρ_p) and the fluid viscosity (μ) on the gas-fluidization behavior. Taking into account that the precursor material has a density of 4800 Kg/m^3 and that Ar was used as carrier gas, the powder shows a SFE (solidlike-to-fluidlike-elutration) behavior from the gas viscosity point of view. With regard to the density of the carrier gas, the powder is classified as Group C of cohesive material in the Geldart diagram (dotted line in Fig. 1). Therefore, the sum of both behaviors results in a highly cohesive precursor powder that can be fluidized under certain circumstances such as centrifugation, by covering the particles with a second material, or by vibration [45, 46, 47]. For that reason a new portable, modular, autonomous, and automated feeder for ultrafine powders has been developed, built and tested in order to achieve the normal fluidization of the powder (Fig. 3). This is an extremely difficult task because the interparticle forces are greater than those that the fluid can exert on the particles [48, 49]. These interparticle forces (Van der Waals, capillary and electrostatic forces) are attractive and higher than particle weight, causing the formation of aggregates, which are difficult to be dragged by the gas stream. In order to achieve a complete fluidization of the cohesive powder these agglomerates have to be broken [50, 51]. This task has been done by providing an additional energy to the particles in the form of waves of ultrasonic frequency [52 - 54]. This piezoceramic was powered by an amplificator system. Besides, the system can work with triangle, square and sinusoidal signals. In a previous step to desagglomeration, the powder was preheated in order to reduce its moisture level. Moreover, a fine jet of powder was achieved using a micro-injector. The bi-phasic fluid (gas + powder) mass flows used in all experiments were: 10 mg/s for the powder and 1.9 l/min for the Ar gas.

As the objective of the work is achieving lines as fine as possible, the injection of the powder was made from the side of the laser beam where the micro-clad is being formed. This geometry ("over hill") is less effective than the opposite one [55]. Saving of precursor powder is achieved as the same time due to the extremely low mass flow ratios used, in the mg/s range, which are 3 orders of magnitude smaller than the typical ones used in conventional laser cladding.

The range of the main processing parameters explored during the tests is summarized in Table 3.

Table 3. Main processing parameters.

Processing parameter	Value
Powder mass flow (mg/s)	10
Conveying gas (l/min)	1.9
Shielding gas (l/min)	20
Nozzle angle (°)	40 - 60
Mean particle size (µm)	8
Laser mean power (W)	30, 40, 50
Laser irradiance (MW/cm^2)	38, 51, 64
Processing speed (mm/s)	0.5 – 40.0
Substrate temperature (^{0}C)	25 - 200

2.4. Characterization techniques

As mentioned in section 2.1, as received powders were characterized by means of X-ray fluorescence (XRF) taken by a Siemens SRS 3000 unit.

Optical microscopy (Nikon Optiphot) was used to measure all micro-clads produced. Figure 4 illustrates the main dimensions of the strips evaluated in this work. The samples were also observed and geometrically characterized by means of an optical interferometric profilometer Wyku-NT1100, working in VSI (vertical scanning interferometry) mode, with a resolution below 1nm and a total working range of 2 mm.

Samples were cut, embedded in acrylic resin and polished to examine the cross-section. The microstructure was also studied by means of scanning electron

microscopy (SEM, Philips XL30) employing a backscattering electron detection mode. The qualitative elemental composition was determined via Energy-dispersive X-ray spectroscopy (EDS, EDAX PV9760 coupled to the SEM).

Due to the small dimensions of the deposited lines, nanoindentation (Nanoindenter II from MTS) was used to determine both Elastic Modulus and Hardness. Nanoindentation involved making a small indentation in the material with a diamond Berkovich indenter while continuously recording the indentation load and the displacement during one complete cycle of loading and unloading. Loads applied ranged from 20 nN to 120 nN and penetrations between 0.1 to 1 micrometre. Due to the small size of the clad, only one indentation per clad was performed, because it is necessary to keep a minimum distance of 50 μm between indentations to prevent the influence from one indentation to the next.

3. RESULTS AND DISCUSSION

3.1. Identification of key parameters by a Design of Experiments (DoE) approach

A 2^4 Full Factorial Design (FDD) was elaborated to identify the key processing parameters with statistical influence on the response variables: width (W), height (H), and penetration (H_2) of the clads [56]. The processing parameters selected as variables for this study were the laser irradiance (I), the processing speed (v), the nozzle angle (α) and the substrate temperature (T). Two levels (designated "+" and "−") for each of the four processing parameters were investigated (see Table 4). For all the tests, the powder mass flow, and the conveying and shielding gases were kept constant at 10 mg/s, 1.9 l/min and 20 l/min respectively. An analysis of the variance (ANOVA) was performed to find out which are the most statistically significant factors on the response variables. Then, a regression model was calculated to analyse the factorial design.

Table 5 summarizes the ANOVA results for the width, height and penetration (only factors with $p < 0.05$ are considered significant).

Table 4. Processing parameters with corresponding levels for the 2^4 FDD.

Processing parameter	Value	
	+	-
(I) Laser irradiance (MW/cm²)	51	64
(v) Processing speed (mm/s)	1	5
(α) Nozzle – substrate angle (°)	40	60
(T) Substrate temperature (°C)	25	200

The ANOVA shows I, v, α, T and the interactions Iv, Iα, vα, IvαT as statistically significant on the width. The height is mainly influenced by I, v, and T. On the contrary, the penetration is mainly influenced by I, v, α and the interactions Iv, Iα from an statistical point of view.

Table 5. ANOVA for width, height and penetration (DF = degree of freedom, SS = sum of squared deviation, V = variance, F = F-ratio, P = P-value). Statistically significant parameters were highlighted in bold format

Width						Height					
	DF	**SS**	**V**	**F**	**p**		**DF**	**SS**	**V**	**F**	**p**
I	**1**	**3102.75**	**3102.75**	**1291.3**	**0**	**I**	**1**	**145.78**	**145.8**	**49.83**	**0**
v	**1**	**5663.14**	**5663.14**	**2356.88**	**0**	**v**	**1**	**3106.69**	**3107**	**1062**	**0**
α	**1**	**23.63**	**23.63**	**9.84**	**0.006**	α	1	6.75	6.75	2.31	0.148
T	**1**	**45.36**	**45.36**	**18.88**	**0.001**	**T**	**1**	**27.94**	**27.94**	**9.55**	**0.007**
I·v	**1**	**20.96**	**20.96**	**8.72**	**0.009**	I·v	1	8.3	8.3	2.84	0.111
I·α	**1**	**18.45**	**18.45**	**7.68**	**0.014**	I·α	1	0.63	0.63	0.22	0.648
I·T	1	0.23	0.23	0.09	0.762	I·T	1	2.26	2.26	0.77	0.393
v·α	**1**	**27.94**	**27.94**	**11.63**	**0.004**	v·α	1	3.06	3.06	1.05	0.321
v·T	1	0.23	0.23	0.09	0.762	v·T	1	6.75	6.75	2.31	0.148
α·T	1	0.58	0.58	0.24	0.631	α·T	1	0.02	0.02	0.01	0.943
I·v·α	1	0.38	0.38	0.16	0.695	I·v·α	1	1.49	1.49	0.51	0.486
I·v·T	1	7.7	7.7	3.21	0.092	I·v·T	1	0.01	0.01	0	0.959
I·α·T	1	0.48	0.48	0.2	0.662	I·α·T	1	0.23	0.23	0.08	0.784
v·α·T	1	2.48	2.48	1.03	0.325	v·α·T	1	0.02	0.02	0.01	0.943
I·v·α·T	**1**	**13.91**	**13.91**	**5.79**	**0.029**	I·v·α·T	1	0.11	0.11	0.04	0.847
Error	16	38.45	2.4			Error	16	46.81	2.93		

Total	31	8966.67			

Total	31	3356.84			

Penetration					
	DF	**SS**	**V**	**F**	**p**
I	**1**	**64.184**	**64.1844**	**131.01**	**0**
v	**1**	**14.797**	**14.7968**	**30.2**	**0**
α	**1**	**2.453**	**2.4531**	**5.01**	**0.04**
T	1	0.49	0.4901	1	0.332
I·v	**1**	**4.56**	**4.5602**	**9.31**	**0.008**
I·α	1	0.987	0.987	2.01	0.175
I·T	1	0.054	0.0544	0.11	0.743
v·α	**1**	**4.396**	**4.3956**	**8.97**	**0.009**
v·T	1	0.097	0.0968	0.2	0.663
α·T	1	0.865	0.8646	1.76	0.203
I·v·α	1	0.063	0.063	0.13	0.725
I·v·T	1	0.072	0.0722	0.15	0.706
I·α·T	1	0.6	0.5995	1.22	0.285
v·α·T	1	0.143	0.1431	0.29	0.596
I·v·α·T	1	0.788	0.7875	1.61	0.223
Error	16	7.839	0.4899		
Total	31	102.387			

Figures 5 and 6 show the graphical response for the main geometrical features of the clads, based on the following regression equations (Eq. 1-3):

$$W(\mu m) = -18.4 + 1.442I - 13.4v - 0.184\alpha - 0.467T + 0.173Iv + 0.0078I\alpha + 0.00862IT + 0.262v\alpha + 0.1344vT + 0.01091\alpha T - 0.00568Iv\alpha - 0.00247IvT - 0.000195I\alpha T - 0.00317v\alpha T + 0.000058Iv\alpha T \quad (1)$$

$$H(um) = 32.3 - 0.025I - 8.6v - 0.522\alpha - 0.080T + 0.072Iv + 0.0106I\alpha + 0.00102IT + 0.115v\alpha + 0.0175vT + 0.00182\alpha T - 0.00225Iv\alpha - 0.00025IvT - 0.000030I\alpha T - 0.00031v\alpha T + 0.000005Iv\alpha T \quad (2)$$

$$H2(um) = -23.8 + 0.437I + 5.13v + 0.418\alpha + 0.067T - 0.0703Iv - 0.00567I\alpha - 0.00106IT - 0.1231v\alpha - 0.0405vT - 0.00107\alpha T + 0.00189Iv\alpha + 0.000731IvT + 0.000017I\alpha T + 0.000755v\alpha T - 0.000014Iv\alpha T \quad (3)$$

Regarding to the width of the clads (see Eq. 1 and Fig. 5.a), this increases with the laser irradiance, but decreases with the processing speed as expected [55]. In the case of the height of the clads, this grows when the laser irradiance increases and the

processing speed decreases (see Fig 5.b). The increment of the processing speed (for a fixed laser irradiance) is more influencing than the increment of the laser irradiance (for a fixed processing speed). If the clad height is evaluated for the different processing speeds (from 5 to 1 mm/s) for a given laser irradiance (51 MW/cm2), the height clad grows from 7 to 25 µm. Analogously, the evaluation for the different laser irradiance (from 51 to 64 MW/cm2) with the same processing speed (5 mm/s) only results in a height clad increasing from 7 to 10 µm. Taking these results in percentage values, it can be observed a gain of 43 % in the clad width with the increase of the laser irradiance, while the height has experienced an increase of 250 % with the processing speed.

On the other hand, the increment of the laser irradiance (for fixed values of the processing speed, and nozzle angle) substantially increases the penetration (see Eq. 3 and Fig. 6). This result is in agreement with those obtained for the dilution in conventional laser cladding (penetration and geometrical dilution are clearly correlated) [55]. Moreover, as the nozzle angle increases, the clad penetration grows. This effect is less notorious as the laser irradiance raises. A possible explanation for the little influence of the nozzle angle parameter could be the extreme precision required by the processing head. On one hand, the irradiated area of the substrate is very small (around 80 μm^2), and on the other hand, the jet of particles of precursor material has low section (around 120 μm^2), and therefore, if the jet of particles is not directed with high accuracy toward the interaction zone, no clad is obtained.

3.2. Establishing the processing parameters map

The results of the factorial DoE allow identifying the laser irradiance and the processing speed as the most influential parameters of the system. Other parameters also have some influence, but it is more restricted as deduced from the ANOVA and regression analyses. These results confirm for laser micro-cladding what has been observed for conventional laser cladding and ratified by several researchers with different materials both in coaxial and off-axis powder injection [55, 57- 60].

Having a clear objective to explore the limits of the laser micro-cladding technique for production of small strips as thin and narrow as possible, efforts were concentrated just on these two parameters. Therefore a more thorough study, broadening the range of values explored, for just laser irradiance and processing speed, and following the "one parameter varied at a time" approach was carried out.

Figure 7 shows the evolution of the clad width as a function of the processing speed and for three different irradiance levels. Micro-clad width increases with the irradiance, whereas it decreases as the values of the processing speed raise. A possible explanation for this behavior could be the following: An increase of the laser irradiance, keeping constant the rest of the processing parameters, results in an increase of the exposure of the substrate to the laser radiation (the area is irradiated the same time with a larger amount of energy), leading to the formation of a bigger molten pool and a higher amount of precursor particles melted, resulting in a broader clad width.

On the other hand, the increase of the processing speed, keeping constant the rest of the processing parameters, has the opposite effect: the exposure of the substrate to the laser radiation is reduced. Therefore, an increase of the processing speed leads to a melt pool of reduced dimensions. Assuming that the amount of precursor particles reaching the interaction zone is not significantly changed, the width of the clad track will be also reduced.

When the processing speed values are too high, the amount of precursor particles melted and adhering to the substrate is not enough to produce a sound clad strip.

The clad width values are in almost all experiments below 80 µm, reaching values smaller than 20 µm for high processing speeds.

With regard to the clad height, the obtained values are in almost all cases below 35 µm, as shown in Fig. 8. The explanation of the clad height behavior with the processing parameters is analog to the case of the clad width: increasing the irradiance means that more particles are melted leading to higher height values whereas increasing the processing speed has the opposite effect.

Both in the case of the clad width and height, two different regions can be identified. For an irradiance of 38 MW/cm^2 the micro-clad tracks are obtained for processing speed values starting at 6 mm/s and up to relative high values of 25.5 mm/s. On the other hand, for higher irradiance values (51 and 64 MW/cm^2), micro-clads are obtained only for processing speeds values below 8 mm/s. This behavior could be due to the fact that higher processing speed values promote an increase in the dilution of the substrate, due to the less amount of precursor particles melted. This argument can be corroborated by the observation of the micro-strips in cross-section as those shown in Fig. 9. Micro-clads are obtained for low processing speed values (Fig. 9.a); whereas increasing the processing speed leads to a micro-alloying area (Fig. 9.c), characterized by a high dilution of the precursor powder material on the substrate [61].

The geometrical dilution ($h_2/(h+h_2)$) analysis plotted in Fig. 10 allows distinguishing between micro-cladding and micro-alloying clads. For an irradiance of 38 MW/cm^2 and high processing speed (between 7 and 26 mm/s), the dilution is, in general, below 20% (micro-cladding clads). For higher irradiance values the dilution reaches values above 50 % when the processing speed is higher than 4 mm/s (micro-alloying clads).

These experiments allow calculating the powder catchment efficiency of the system, resulting on a mean value of 1,3 %. This value is in accordance with the studies of Partes [62] that shows a decrease in the catchment efficiency with the molten pool size. Besides, it should be taken into account that the mean value of precursor powder used during the formation of each micro-clad is only 165 mg.

Figure 11 collects SEM micrographs of cross-section views of micro-clads obtained under different conditions. This kind of map illustrates the dependence of the geometrical features (width, height and penetration) with the main parameters of the micro-cladding process: processing speed and laser irradiance. Similar behavior to the one obtained by conventional cladding process is clearly observed [59], having the thickest micro-clads for the highest irradiance values and lowest processing speeds. Keeping the processing speed constant, smaller clads in width and height will be produced by decreasing the laser irradiance. On the other hand, the increase in the

processing speed, with the same irradiance level, allows obtaining clads with smaller dimensions.

Figure 12 collects all results previously shown and also those leading to discontinuous clads, resulting in the processing parameters map of laser micro-cladding. As shown in this figure, different regions can be identified in terms of the type of strip obtained. First, for the lowest processing speed values, there is a region where tracks are not obtained. In this case all the energy delivered by the laser beam is used in melting the precursor particles but not the substrate. The excessively high lineal energy (laser mean power per processing speed, P/v) in this region, promotes the formation of a succession of consecutive spheres made out of molten powder due to the superficial tension [63], instead of continuous clads. Increasing the processing speed opens a micro-cladding working window, where clad strips in the range of micrometres are obtained both in width and height. A further increase in the processing speed leads to a region of micro-alloying, characterized for high grade of dilution of the strips, due to the high amount of molten substrate material. Finally, the highest processing speeds promote the formation of discontinuous clads, because the lineal energy is not high enough to produce a continuous melting pool.

3.3. Micro-clads obtained under optimal conditions

Once the working window has been identified for laser micro-cladding of Co-superalloy, the goal was to obtain strips as thin and narrow as possible. Among all the processing parameter values tested in the experiments, the combination of a laser irradiance of 38 MW/cm^2 and a processing speed of 18 mm/s has proved to be the optimal processing parameters, allowing to produce micro-clad tracks with minimum width value of 14 µm, height of only 7.2 µm, low dilution and negligible heat affected zone. Figure 13 shows an example of one of these optimal micro-clad tracks produced in the experiments.

Dimensional stability of the micro-cladding process was assessed by producing several parallel strips under the optimal processing conditions. Fig. 14.a, obtained by means of

3D optical surface profilometry, shows a representative example of the superficial aspect of the micro-clads obtained in the tests. It can be observed the high dimensional stability of the clad tracks along all their length. Fig. 14.b shows one the strips more in detail. Moreover, the mean roughness of the micro-clads has been measured, having obtained a value of 1.83 μm against the 0.16 μm of the substrate. This increase in the surface roughness is due to the presence of microparticles from the precursor powder that have been only partially molten as can be observed under the SEM (see Fig. 15).

3.4. Mechanical properties and microstructure

Once obtained the smallest clad strips achievable with this system, a remaining aspect are the mechanical properties of the deposited material.

Regarding the hardness, Fig. 16 plots the changes in the hardness of the micro-clads with the displacement of the nano-indenter inside the material. Hardness of the micro-clads tends to stabilize quickly and becomes independent of the indentation depth with values between 10 and 8 GPa. These values are 4-5 times higher than the hardness of the initial powder. This increment could well be due to the extremely fast cooling that takes place during the process. But a certain contribution could be also due to the indentation size effect [64].

With regard to the Elastic Modulus, measured values of micro-clad Young's moduli have shown results between 231 and 221 GPa. These values are similar to those reported in the literature for co-superallloys clads over steel produced by conventional laser cladding technique [65]. This result is indicative of a low dilution of the substrate in the coating.

Regarding to micro-clad microstructure, a typical example can be seen in Fig. 17.a. It can be emphasized that the heat affected zone has a negligible size due to the fact that laser irradiation takes place in a very small area of the substrate. On the other hand, the microstructure analysis of the transversal section of the micro-clads reveals the presence of a preponderant phase of α-Co dendritic grains, and an eutectic phase of

cobalt and carbides (Cr, W and Co) of high hardness (see Fig. 17.b), distinctive of laser cladding process with cobalt alloys over steel [59, 66, 67]. The presence of these carbides could well be responsible for the high hardness measured on the micro-clad strips. The EDS analysis revealed that the carbides are M_7C_3 type, with M = Co, Cr or W [68-71]. Moreover, no specific dendritic growth direction has been observed. The boundary layer between the micro-clad and the substrate is clearly continuous, without porous and free of cracks (Fig. 12.c), which is an indicative of a good adhesion [59, 66]. The micro-clad zone closest to the substrate, with a thickness about 1 μm, has a clear planar solidification without interdendritic phases, as it could be expected [72]. However, the zone of the clad microstructure that should show a columnar dendritic growth is not easily observed, only a slight elongation of the grains in the perpendicular direction to the solidification front can be observed. This fact could be due to two possible phenomena. Firstly, due to the reduced height of the micro-clad, the usual conditions for a preferential dendritic growth direction, i.e.: a high temperature gradient in the clad, do not occur. Secondly, the grain size of the micro-clads obtained is smaller than the analog one in conventional laser cladding. In general, the mean grain size in laser cladding is about 90 μm, within a range from 20 up to 180 μm [65, 73], whereas the SEM micrographs of the micro-clads produced by laser micro-cladding show a mean grain size of 5 μm or less, that results in a more refined microstructure of the micro-clad tracks, not being possible to observe an appreciable elongation of the grains.

4. GENERAL REMARKS

Since the starting of the early works on production of coatings by laser cladding in the early 1980s, efforts have been directed mainly to produce large layers with thickness in the millimetre range and with high deposition rates in the range of several kilograms per hour [16, 57, 58]. The objectives of the technique here used are the opposite, aiming to deposit strips as thin and narrow as possible. To achieve this goal, melt pool has been reduced from tens of millimetres to 10 micrometres. This has been only possible by means of the new generation of high brightness lasers capable to deliver irradiances in the range of the 10^7 W/cm^2 with a good beam quality and at affordable

cost. These values are two orders of magnitude higher than those used in conventional laser cladding [16].

At the same time, the precursor material size has to be also scaled down. From hundreds of micrometres of average size of powders used in conventional cladding, to the less than 10 μm used in the present work. Using these very small particles poses another challenge: the interparticle forces (Van der Waals, capillary and electrostatic forces) are much stronger than the proper weight of the particles. Therefore the particles stay together forming agglomerates. These agglomerates are so large that existing commercial powder feeders are not useful here. This means that a new, more sophisticated powder feeder is required, adding ultrasonic waves to the kinematic energy transmitted by the gas jet. The new powder feeder here described is able to deliver a mass flow of just milligrams per second, which is 3 orders of magnitude smaller than the nominal mass flow for commercial powder feeders. Application of this powder feeder to other types of powders or substrates different from stainless steel is under research, being the most limiting factor the absorptivity of both powder and substrate to the laser beam, rather than factors related to powder agglomeration or flowing through the injection nozzle.

Production of a thin narrow clad line of material on a substrate requires a fine alignment of the powder nozzle and the laser beam, which contrast with the less restrict alignment of laser beam and powder jet in conventional laser cladding.

This work is just the proof-of-concept for the production of extremely small clads of a Co-superalloy keeping all its good properties. The extremely low heat input transmitted to the substrate encourages the application of this technique to direct-write fine lines on temperature sensible substrates. The ability of producing hard lines on a given substrate allows modifying its surface topography as well as tribologic properties. This can be applied to micro bearings, sliding micro-tracks, or to enhance local wear resistance to clamping flanges or micro-tools. Micro-mould fabrication and repairing, and production of 3D parts at sub-millimetre scale are promising future fields of application of this technique.

The good control of the geometrical features of the strips, the absence of expensive vacuum chambers, and the possibility of depositing small amount of material opens the possibility to produce functional 3D parts at the sub-millimetre range. Obviously, the necessary industrialization of laser head and powder feeder need to be accomplished prior to the application at industrial scale.

5. CONCLUSIONS

Fine lines of Co-superalloy were direct written on AISI 316 stainless steel by side powder injection laser micro-cladding technique.

In order to achieve lines as thin and narrow as possible, while keeping the mechanical properties of deposited layer similar to those of the precursor material, fine precursor powder (main grain size of 8 μm) was used. The small size of the powder implies that commercial powder feeders are useless here. Therefore a new powder feeder was designed, constructed and successfully tested.

A full factorial design of experiments allowed identifying laser irradiation and processing speed as the most influential parameters of the process, corroborating at micrometre scale what was known since many years for conventional laser cladding at millimetre or sub-millimetre scales.

A thorough study of the influence of these two parameters on the main geometrical features of the micro-clads allowed establishing the processing parameters map. Four main zones were identified: a zone where not proper clads are formed (balling), a micro-cladding zone, micro-alloying zone, and a zone were strips are discontinuously formed. It should be pointed out that the working window for the micro-cladding process is rather small.

Under optimized conditions fine lines of Co-superalloy, just 14 μm wide and 7.2 μm thick, were obtained. Strips are dense, crack-free, showing mechanical properties (in terms of hardness and elastic modulus), and microstructure similar to those of the precursor material.

6. ACKNOWLEDGEMENTS

This work was partially supported by the EU research project Bluehuman (EAPA_151/2016 Interreg Atlantic Area), Government of Spain (MAT2015-71459-C2-1-P (MINECO/FEDER)), and by Xunta de Galicia (ED431B 2016/042 (GPC), ED481B 2016/047-0, ED481D 2017/010). Authors wish to thank the technical staff from CACTI (University of Vigo) for their help with sample characterization.

7. REFERENCES

[1] D. J. Ehrlich, J. Y. Tsao, Laser direct writing for VLSI in N. G. Einspruch (Ed.) VLSI Electronics, Microstructure Science Vol.7 Academic Press Inc. ,Orlando, FL, (1983) 129-164.

[2] C. Garrido, D. Braichotte, H. Van den Bergh, B. León, M. Pérez-Amor, Interconnection lines of Pt induced by laser direct writing, Applied Surface Science 43 (1989) 68 -73.

[3] M. Wang, Q. Liu, H. Zhang, C. Wang, L. Wang, B. Xiang, Y. Fan, C. F. Guo, S. Ruan, Laser direct writing of tree-shaped hierarchical cones on a superhydrophobic film for high-efficiency water collection, ACS Applied Materials Interfaces 9 (2017) 29248−29254.

[4] I.-B. Sohna, H.-K. Choia, D. Yooa, Y.-C. Noha, J. Nohb, Md. S. Ahsanc, Three-dimensional hologram printing by single beam femtosecond laser direct writing, Applied Surface Science 427 (2018) 396–400.

[5] S. D. Gittard, R. J. Narayan, Laser direct writing of micro- and nano-scale medical devices, Expert Review of Medical Devices. 7 (2010) 343–356.

[6] W. Xiong, Y. Zhou, W. Hou, L. Jiang, M. Mahjouri-Samani, J. Park, X. He, Y. Gao, L. Fan, T. Baldacchini, J.-F. Silvain, Y. Lu, Laser-based micro/nanofabrication in one, two and three dimensions, Frontiers of Optoelectronics 8 (2015) 351–378.

[7] H N Hansen, K Carneiro, H Haitjema, L De Chiffre, Dimensional Micro and Nano Metrology, CIRP Annals – Manufacturing Technology, 55 (2007) 721 – 741.

[8] M. Vaezi, H. Seitz, S. Yang, A review on 3D micro-additive manufacturing technologies, The International Journal of Advanced Manufacturing Technology, 67 (2013) 1721-1754

[9] B. Su, J. Meng, Z. Zhang, F. Liu, A. Zhang, Fabrication of alumina micromixer with two-dimensional serpentine microchannels by centrifuge-assisted micromoulding, Micro & Nano Letters, 10 (2015) 703–706.

[10] C.A. Griffiths, A. Rees, R.M. Kertona, O.V. Fonseca, Temperature effects on DLC coated micro moulds, Surface & Coatings Technology 307 (2016) 28–37

[11] P. González, D. Fernández, J. Pou, E. García, J. Serra, B. León, M. Pérez-Amor, Photo-induced chemical vapour deposition of silicon oxide thin films, Thin Solid Films 218 (1992) 170-181.

[12] F.-W. Bach, A. Laarmann, T. Wenz, Modern Surface Technology, WILEY-VCH Verlag, Weinheim, 2016.

[13] L. Pawlowski, Thermal Spraying Techniques, in The Science and Engineering of Thermal Spray Coatings, Second Edition, John Wiley & Sons (2008), Ltd, Chichester, UK.

[14] X. Li, H. Li, J. Liu, X. Qi, X. Zeng, Conductive line preparation on resin surfaces by laser micro-cladding conductive pastes, Applied Surface Science 233 (2004) 51–57

[15] F. Lusquiños, R. Comesaña, A. Riveiro, F. Quintero, J. Pou, Fibre laser micro-cladding of Co-based alloys on stainless steel, Surf. Coatings Technol. 203 (2009) 1933–1940.

[16] W.M. Steen, Laser Materials Processing, Springer Verlag, London,2003, p. 254.

[17] A. Riveiro, A. Mejías, F. Lusquiños, J. del Val, R. Comesaña, J. Pardo, J. Pou, Laser cladding of aluminium on AISI 304 stainless steel with high-power diode lasers, Surf. Coatings Technol. 253 (2014) 214–220.

[18] K. Li, D. Li, D. Liu, G. Pei, L. Sun, Microstructure evolution and mechanical properties of multiple-layer laser cladding coating of 308L stainless steel, Applied Surface Science 340 (2015) 143–150.

[19] R. Gassmann, Laser cladding with (WC + W2C)/Co-Cr-C and (WC + W2C)/Ni-B-Si composites for enhanced abrasive wear resistance, Materials Science & Technology 12 (1996) 691–696.

[20] L. Shepeleva, B. Medres, W.D. Kaplan, M. Bamberger, A. Weisheit, Laser cladding of turbine blades, Surf. Coatings Technol. 125 (2000) 45–48.

[21] F. Arias-González, J. del Val, R. Comesaña, J. Penide, F. Lusquiños, F. Quintero, A. Riveiro, M. Boutinguiza, J. Pou, Fiber laser cladding of nickel-based alloy on cast iron, Appl. Surf. Sci. 374 (2016) 197–205.

[22] F. Arias-González, J. del Val, R. Comesaña, J. Penide, F. Lusquiños, F. Quintero, A. Riveiro, M. Boutinguiza, J. Pou, Laser cladding of phosphor bronze, Surface & Coatings Technology 313 (2017) 248–254.

[23] K. Watkins, M. McMahon, W. Steen, Microstructure and corrosion properties of laser surface processed aluminium alloys: a review, Materials Science & Engineering A. 231 (1997) 55–61.

[24] Y. Diao, K. Zhang, Microstructure and corrosion resistance of TC2 Ti alloy by laser cladding with Ti/TiC/TiB2 powders, Applied Surface Science 352 (2015) 163–168.

[25] A. Kurella, N.B. Dahotre, Laser induced hierarchical calcium phosphate structures, Acta Biomaterialia 2 (2006) 677–683.

[26] M. Roy, B. Vamsi Krishna, A. Bandyopadhyay, S. Bose, Laser processing of bioactive tricalcium phosphate coating on titanium for load-bearing implants, Acta Biomaterialia 4 (2008) 324–333.

[27] R. Comesaña, F. Lusquiños, J. del Val, M. López-Álvarez, F. Quintero, A. Riveiro, M. Boutinguiza, A. De Carlos, J.R. Jones, R.G. Hill, J. Pou, Three-dimensional bioactive glass implants fabricated by rapid prototyping based on CO2 laser cladding, Acta Biomaterialia, 7 (2011) 3476-3487.

[28] T.H. Kim, J.H. Chung, Fabrication of Functionally Gradient Materials in Inconel/Steel System by Laser Beam, Materials Transactions JIM. 38 (1997) 1010–1015.

[29] J. del Val, R. Comesaña, F. Lusquiños, M. Boutinguiza, A. Riveiro, F. Quintero, et al., Laser cladding of Co-based superalloy coatings: Comparative study between Nd:YAG laser and fibre laser, Surface & Coatings Technology 204 (2010) 1957–1961.

[30] F. Lusquiños, J. Pou, F. Quintero, M. Pérez-Amor, Laser cladding of SiC/Si composite coating on Si–SiC ceramic substrates, Surface & Coatings Technology 202 (2008) 1588–1593.

[31] H. Li, X. Zeng, H. Li, Study on thick film resistor and electrode fabricated by laser micro-cladding electronic pastes, Surface & Coatings Technology 200 (2006) 6832.

[32] H. Li, X. Zeng, Study on the structure and properties of thick-film capacitors fabricated by laser micro-cladding and rapid prototype, Journal of Materials Processing Technology 184 (2007) 184–189.

[33] T. Jambor, K. Wissenbach, Proceedings of the Fourth International WLT-Conference on Lasers in Manufacturing, Munich, Germany, 2007, p. 193.

[34] C. Jimin, Z. Tiechuan, Journal of Laser Applications 16 (2004) 258.

[35] S. N. Grigoriev, T. V. Tarasova, G. O. Gvozdeva, St. Nowotny, Microcladding of hypereutectic Al–Si alloys: technological aspects and structure features, International Journal of Cast Metals Research 27 (2014) 357.

[36] S.N. Grigoriev, T.V. Tarasova, G.O. Gvozdeva, St. Nowotny, Solidification behaviour during laser microcladding of Al–Si alloys, Surface & Coatings Technology 268 (2015) 303–309.

[37] B. Yao, X.L. Ma, F. Lin, W.J. Ge, Microstructure and mechanical properties of Ti-6Al-4V components fabricated by laser micro cladding deposition, Rare Metals 34 (2015) 445–451.

[38] F. Brueckner, M. Riede, F. Marquardt, R. Willner, A. Seidel, S. Thieme, C. Leyens, E. Beyer, Process characteristics in high-precision laser metal deposition using wire and powder, Journal of Laser Applications29 (2017) 022301/6.

[39] A.G. Demir, Micro laser metal wire deposition for additive manufacturing of thin-walled structures, Optics and Lasers in Engineering 100 (2018) 9–17.

[40] P. Regenfuss, A. Streek, L. Hartwig, S. Klötzer, Th. Brabant, M. Horn, R. Ebert, H. Exner, Principles of laser micro sintering, Rapid Prototyping Journal, 13 (4) (2007) 204-212.

[41] H. Exner, M. Horn, A. Streek, F. Ullmann, L. Hartwig, P. Regenfuß, R. Ebert Laser micro sintering: A new method to generate metal and ceramic parts of high resolution with sub-micrometer powder, Virtual and Physical Prototyping, 3:1 (2008) 3-11.

[42] A.G. Demir, B. Previtali, Additive manufacturing of cardiovascular CoCr stents by selective laser melting, Materials and Design 119 (2017) 338–350.

[43] J. Del Val, R. Comesaña, F. Lusquiños, A. Riveiro, F. Quintero, J. Pou, Downscaling of conventional laser cladding technique to microengineering, Physics Procedia 5 (2010) 341–348.

[44] J.R. Davis, Nickel, Cobalt, and Their Alloys, ASM International, Materials Park, OH, 2000.

[45] D. Geldart, The effect of Particle Size and Size Distribution on the Behaviour of Glass-Fluidised Beds, Powder Technology 6 (1971) 201 – 215.

[46] D. Geldart, Types of gas fluidization, Powder Technology 7 (1973) 285

[47] J.M. Valverde, A. Castellanos, Extension of Geldart's Diagram to Fluidizable Fine and Ultrafine Particles, AIP Conference Proceedings 1145 (2009) 977 – 980.

[48] J.P.K. Seville, C.D. Willet, P.C. Knight, Interparticle forces in fluidization: a review, Powder Technology 113 (2000) 261 – 268.

[49] D.P. Debrincat, C.B. Solnordal, J.S.J. Van Deventer, Characterisation of inter-particle forces within agglomerated metallurgical powders, In Powder Technology, 182 (2008) 388-397.

[50] S. Matsusaka, M. Urakawa, H. Masuda, Micro-feeding of fine powder using a capillary tube with ultrasonic vibration, Advanced Powder Technology,6 (1995) 283 – 293.

[51] M. Mracek, J. Wallaschek, A system for powder transport based on piezoelectrically excited ultrasonic progressive wave, Materials Chemistry and Physics 90 (2005) 378 – 380.

[52] Y. Yang, X. Li, Experimental and analytical study of ultrasonic micro power feeding, Journal of Physics D: Applied Physics 36 (2003) 1349 – 1354.

[53] X. Lu, S. Yang, J.R.G. Evans, Studies on ultrasonic microfeeding of fine powders, Journal of Physics D: Applied Physics, 39 (2006) 2444-2453.

[54] L. Qi, X. Zeng, J. Zhou, J. Luo, Y. Chao, Stable micro-feeding of fine powders using a capillary with ultrasonic vibration, Powder Technology, 214 (2011) 237 – 242.

[55] U. de Oliveira, V. Ocelík, J.Th.M. De Hosson, Analysis of coaxial laser cladding processing conditions, Surf. Coatings Technol. 197 (2005) 127-136.

[56] D.C. Montgomery. Design and Analysis of Experiments, 8th Edition, John Wiley & Sons, 2012.

[57] V. M. Weerasinghe, W. M. Steen, Laser cladding with pneumatic powder delivery, in Applied Laser Tooling, edited by O. D. D. Soares and M. Perez-Amor, Nijhoff, Dordrecht, 1987, pp. 183–212.

[58] R. Vilar, Laser cladding, Journal of Laser Applications 11 (1999) 64.

[59] V. Ocelík, U. de Oliveira, M. de Boer, J.T.M. de Hosson, Thick Co-based coating on cast iron by side laser cladding: Analysis of processing conditions and coating properties, Surface & Coatings Technology 201 (2007) 5875–5883.

[60] F. Lusquiños, J. Pou, M. Boutinguiza, F. Quintero, R. Soto, B. León, M. Pérez-Amor, Main characteristics of calcium phosphate coatings obtained by laser cladding, Applied Surface Science, 247 (2005) 486-492.

[61] F. Lusquiños, J. Pou, J.L. Arias, M. Boutinguiza, B. León, M. Pérez-Amor, F.C.M. Driessens, Alloying of hydroxyapatite onto Ti6Al4V by high power laser irradiation, Journal of Materials Science: Materials in Medicine, 13 (2002) 1-5.

[62] K. Partes, Analytical model of the catchment efficiency in high speed laser cladding, Surface and Coatings Technology, 204 (2009) 366-371.

[63] M. Ellis, D.C. Xiao, C. Lee, W.M. Steen, K.G. Watkins, W.P. Brown, Processing aspects of laser cladding an aluminium alloy onto steel, Journal of Materials Processing Technology, 52 (1995) 55-67.

[64] K.W. McElhaney, J.J. Vlassak, W.D. Nix, Journal of Materials Resarch 13 (1998) 1300.

[65] U. de Oliveira, V. Ocelík, J.Th.M. De Hosson, Residual stress analysis in Co-based laser clad layers by laboratory X-rays and synchrotron diffraction techniques, Surface & Coatings Technology 201 (2006) 533-542.

[66] D.P. Bykovskiy, V.N. Petrovskiy, P.S. Dzhumaev, V.I. Polskiy, V.M. Yermachenko (2016). Analysis of microstructure and properties of multilayer coatings produced by laser cladding. Journal of Physics: Conference Series, 691 (2016) 012008.

[67] C. Cui, Z. Guo, Y. Liu, Q. Xie, Z. Wang, J. Hu, Y. Yao, Characteristics of cobalt-based alloy coating on tool steel prepared by powder feeding laser cladding, In Optics & Laser Technology, 39 (2007) 1544-1550.

[68] A. Frenk, W. Kurz, High speed laser cladding: solidification conditions and microstructure of a cobalt-based alloy, Materials Science and Engineering, A 173 (1993) 339-342.

[69] A. Frenk, W. Kurz, Microstructural effects on the sliding wear resistance of a cobalt based alloy, Wear, 174 (1994) 81-91.

[70] W.C. Lin, C. Chen, Characteristics of thin surface layers of cobalt-based alloys deposited by laser cladding, Surface & Coatings Technology 200 (2006) 4557 – 4563.

[71] N.I. Medvedeva , D.C. Van Aken, J.E. Medvedeva, Stability of binary and ternary M23C6 carbides from first principles, Computational Materials Science 96 (2015) 159–164.

[72] M Zhong, W Liu, Laser surface cladding: The state of the art and challenges, Proceedings of the Institution of Mechanical Engineers, Part C: Journal of Mechanical Engineering Science 224(2010) 1041

[73] V. Ocelík, I. Furár, J.Th.M. De Hosson, Microstructure and properties of laser clad coatings studied by orientation imaging microscopy, Acta Materialia 58 (2010), 6763 – 6772.

FIGURE CAPTIONS

Figure. 1. SEM micrograph of the precursor powder (a) and its classification according to extended Geldart diagram (b).

Figure 2. Laser head specifically designed and constructed for micro-cladding.

Figure 3. Powder feeder specially designed to fluidizate powder of cohesive nature (a) and block diagram of experimental set-up for laser micro-cladding technique (b).

Figure 4. Geometrical features of the clad strips: width, thickness and penetration depth.

Figure 5. Contour plot of the micro-clad track width (μm) (a) and height (μm) (b) versus the processing speed and the laser irradiance. (nozzle angle and substrate temperature were fixed at α=50° and T=112.5°C in both cases).

Figure 6. Contour plot of the micro-clad track penetration (μm) versus the processing speed and the laser irradiance (a) (nozzle angle and substrate temperature were fixed at α=50° and T=112.5°C). Contour plot of the micro-clad track penetration (μm) versus the nozzle angle and the laser irradiance (b) (processing speed and substrate temperature were fixed at v=3mm/s and T=112.5°C).

Figure 7. Behavior of the clad width as a function of the processing speed and laser irradiance.

Figure 8. Evolution of the clad height as a function of processing speed and laser irradiance.

Figure 9. Evolution of the tracks from micro-cladding (a) to micro-alloying (c). Laser irradiance 64 MW/cm^2, processing speed: 8 mm/s (a), 14 mm/s(b), 20 mm/s (c). Bar scale in all SEM micrographs is 10 μm.

Figure 10**.** Influence of processing speed and laser irradiance on the geometrical dilution.

Figure 11. Cross-section of the micro-clads shown by SEM micrographs for different processing parameters. Note that the mark in every micrograph is 10 micrometres

Figure 12. Processing map for the different combinations of the main laser micro-cladding parameters.

Figure 13**.** Cross-section of a micro-clad produced under optimal processing parameters. (Laser irradiance 38 MW/cm^2, processing speed 18 mm/s, powder mass flow 10 mm/s).

Figure 14. 3D optical suface profilometry of several micro-clad tracks (a). Detail of one of the micro-clad obtained (b).

Figure 15. SEM micrograph of the track surface. Inset shows a detail of the surface at higher magnification.

Figure 16. Mean hardness value as function of the displacement of nanoindenter tip into the material.

Figure 17. SEM cross section micrograph of micrometre clad (a). Detail of the microstructure (b), and detail of the interface substrate-clad (c). (Laser irradiance 51 MW/cm^2, processing speed 3.5 mm/s).

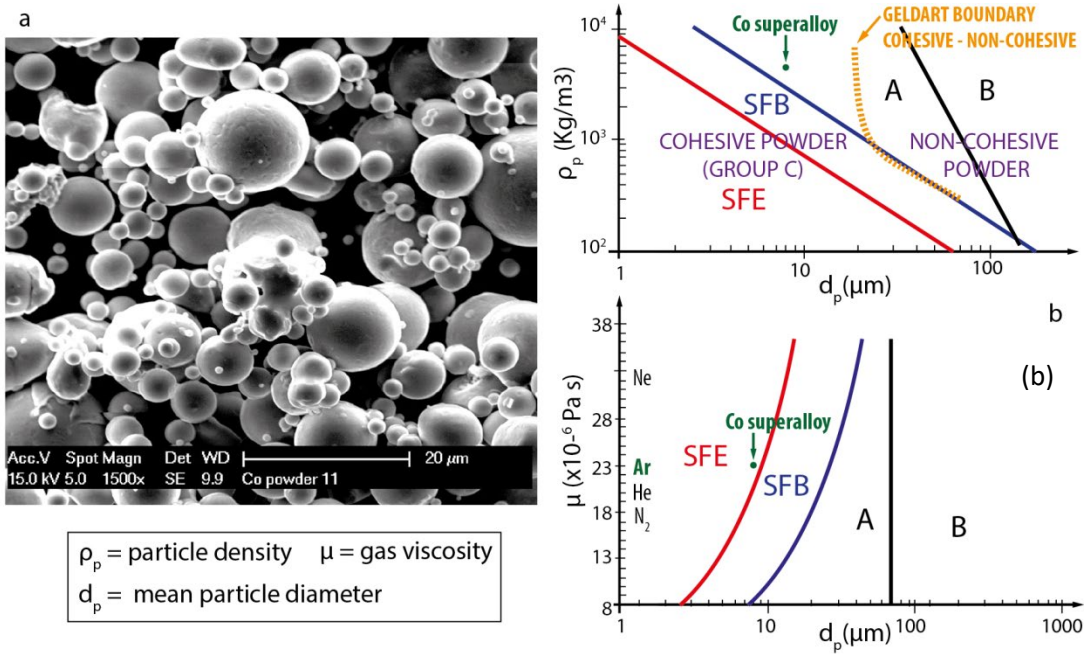

Figure. 1. SEM micrograph of the precursor powder (a) and its classification according to extended Geldart diagram (b).

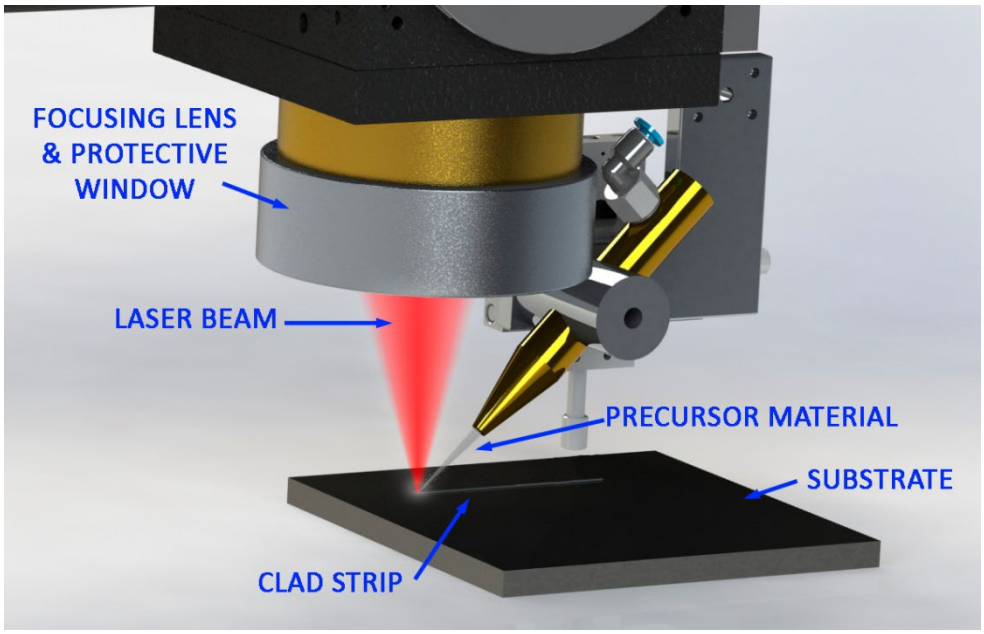

Figure 2. Outline of the laser micro-cladding experimental set-up.

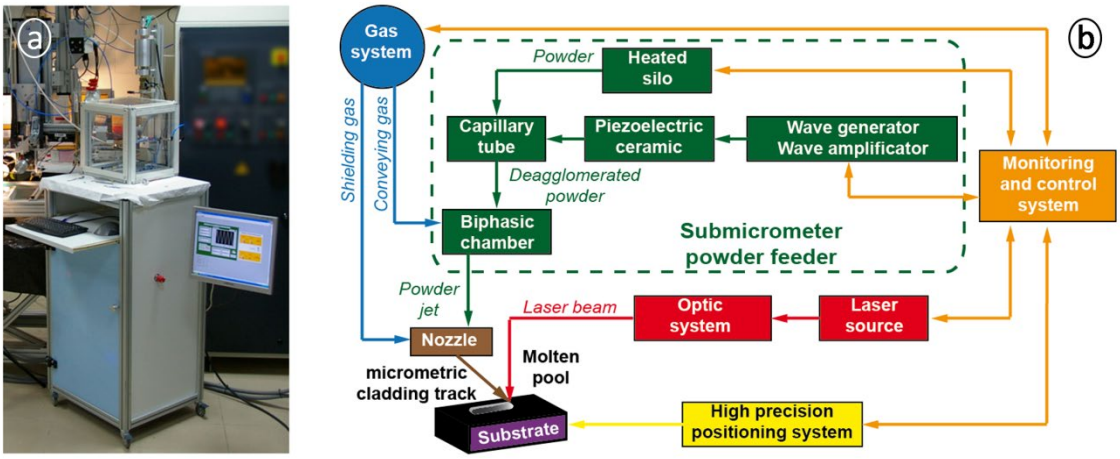

Figure 3. Micro-powder feeder specially designed to fluidizate powder of cohesive nature (a) and block diagram of experimental set-up for laser micro-cladding technique (b).

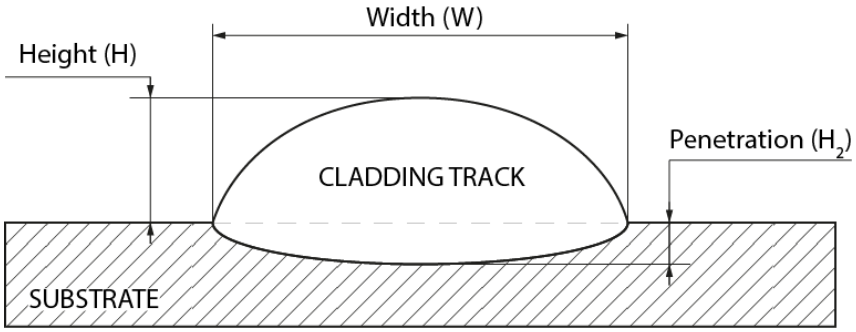

Figure 4. Geometrical features of the clad strips: width, thickness and penetration depth.

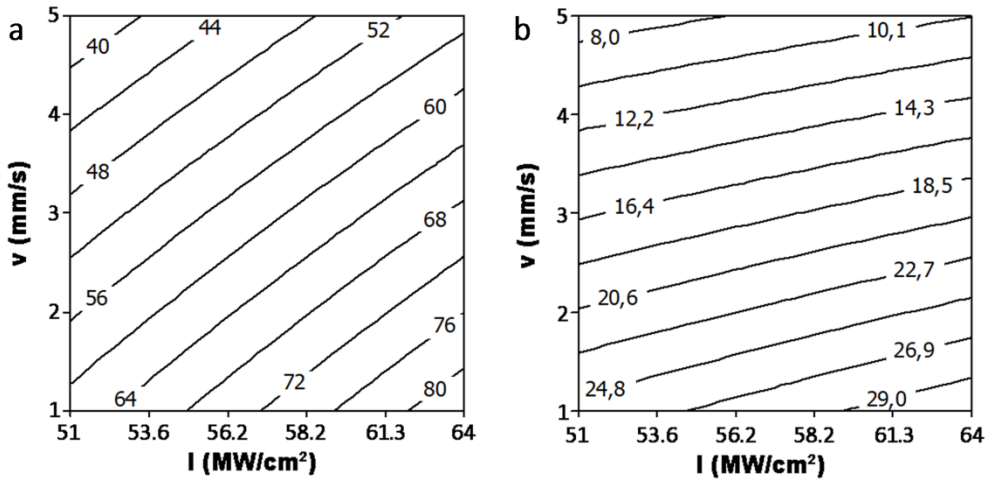

Figure 5. Contour plot of the micro-clad track width (µm) (a) and height (µm) (b) versus the processing speed and the laser irradiance (nozzle angle and substrate temperature were fixed at α=50° and T=112.5°C in both cases).

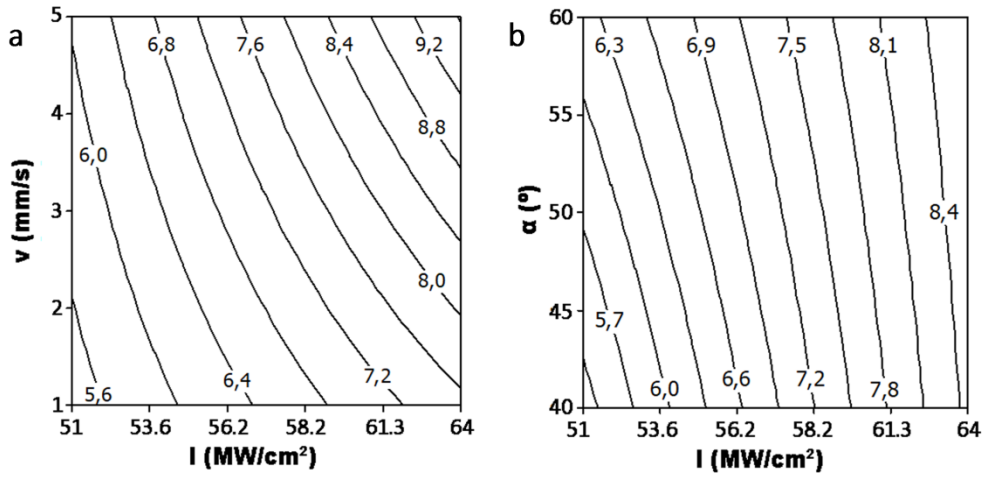

Figure 6. Contour plot of the micro-clad track penetration (µm) versus the processing speed and the laser irradiance (a) (nozzle angle and substrate temperature were fixed at α=50° and T=112.5°C). Contour plot of the micro-clad track penetration (µm) versus the nozzle angle and the laser irradiance (b) (processing speed and substrate temperature were fixed at v=3mm/s and T=112.5°C).

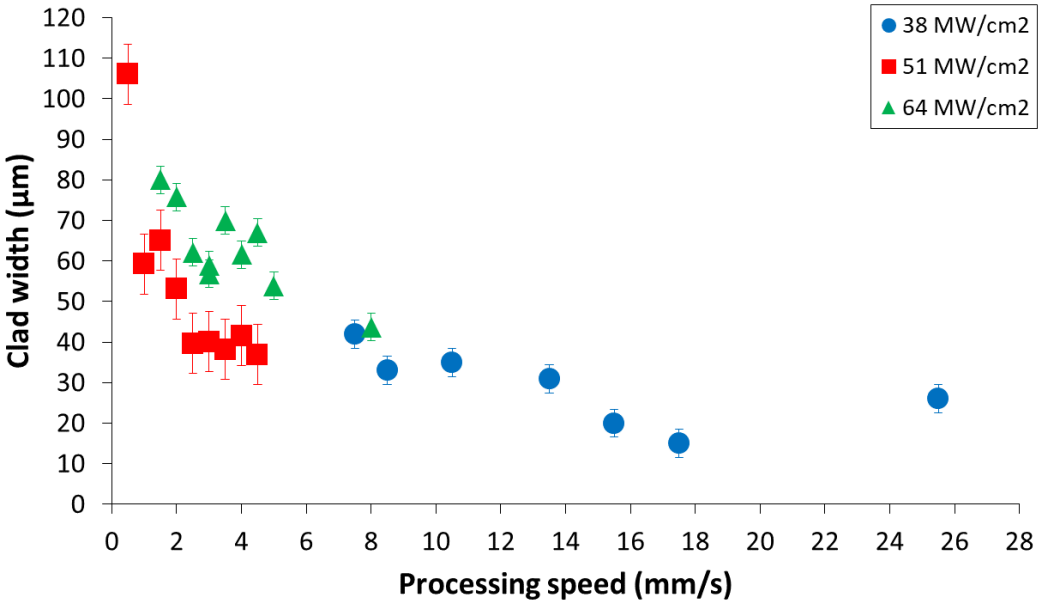

Figure 7. Clad width according to the processing speed and laser mean power (powder mass flow 10 mg/s).

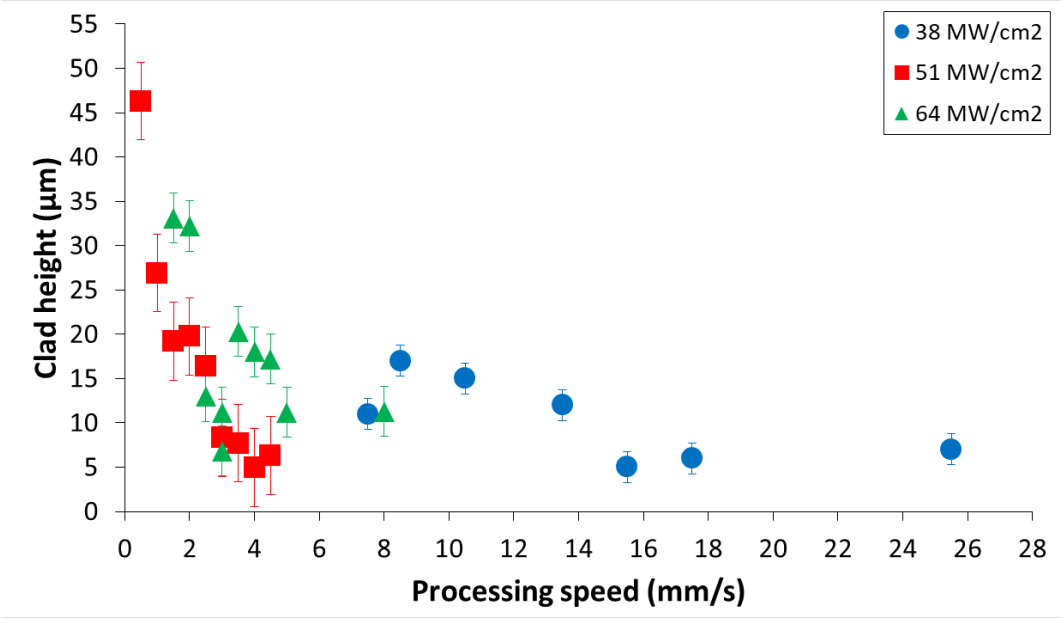

Figure 8. Evolution of the clad thickness according to the processing speed and laser irradiation (powder mass flow 10 mg/s).

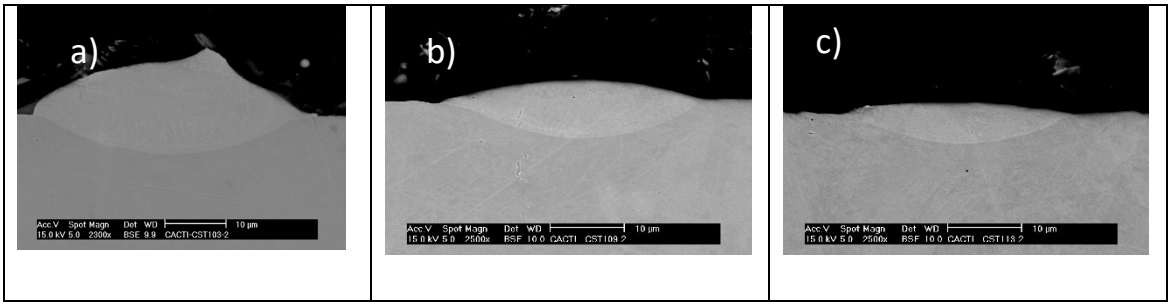

Figure 9. Evolution of the tracks from micro-cladding (a) to micro-alloying (c). Laser irradiance 64 MW/cm^2, processing speed: 8 mm/s (a), 14 mm/s(b), 20 mm/s (c). Bar scale in all SEM micrographs is 10 µm.

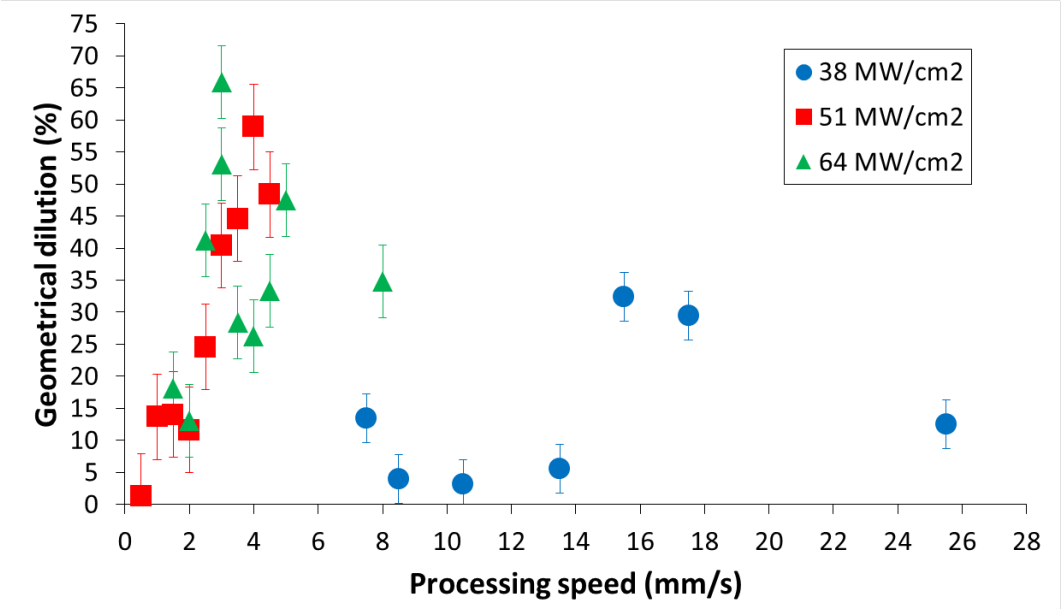

Figure 10. Evolution of the geometrical dilution according to processing speed and laser irradiance (powder mass flow 10 mg/s).

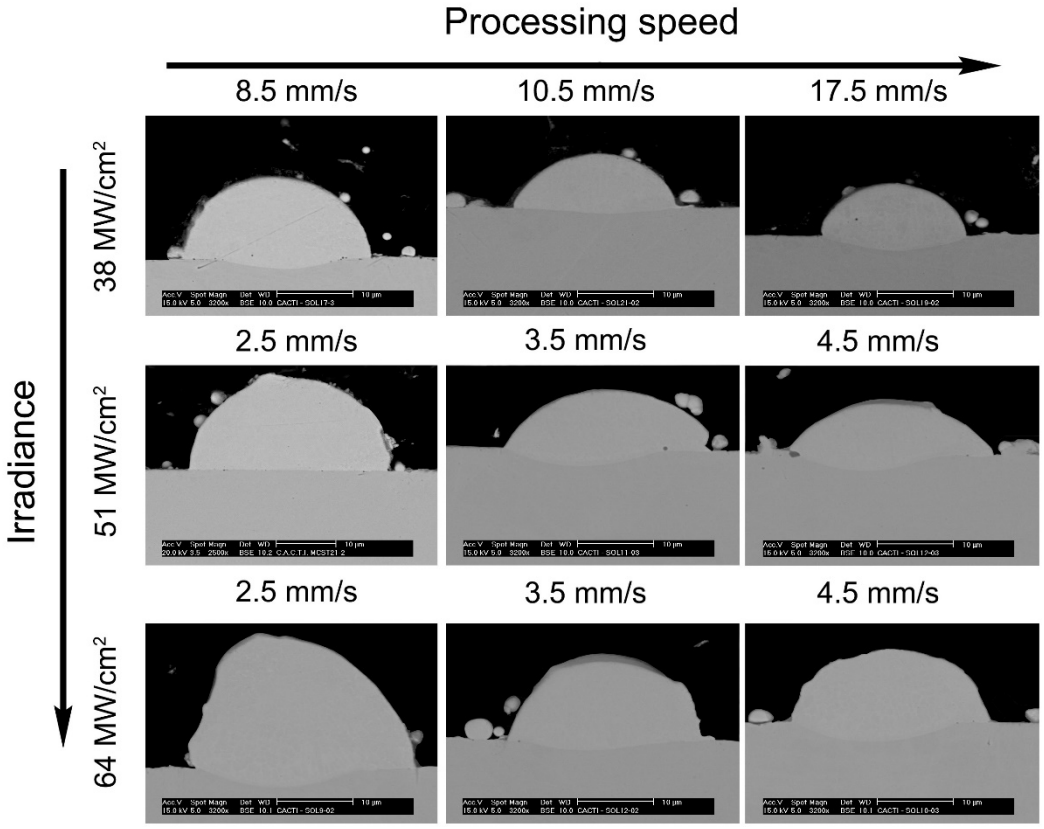

Figure 11. Cross-section of the micro-clads shown by SEM micrographs for different processing parameters (powder mass flow 10 mg/s). Note that the mark in every micrograph is 10 micrometres

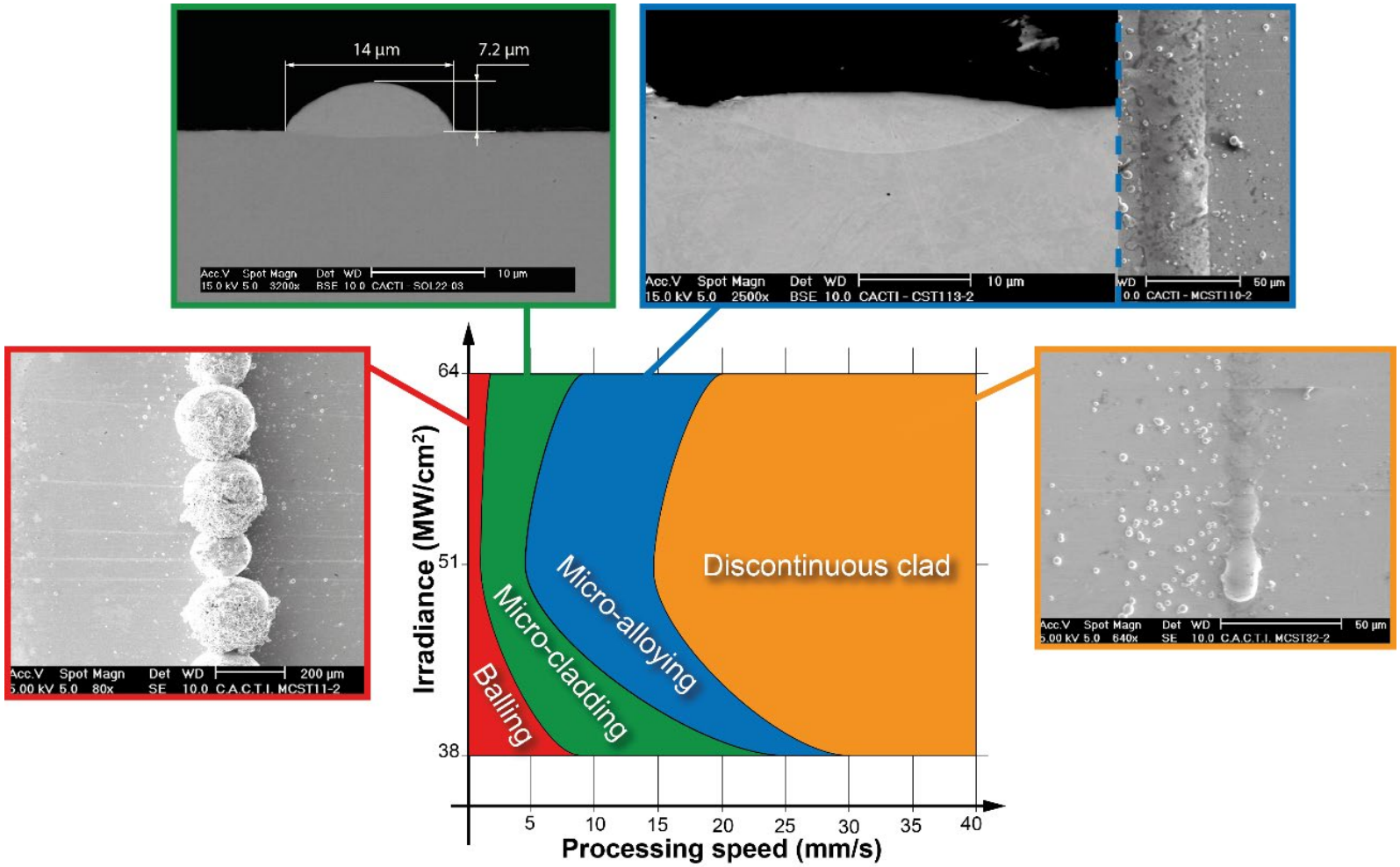

Figure 12. Processing map for the different combinations of the main laser micro-cladding parameters.

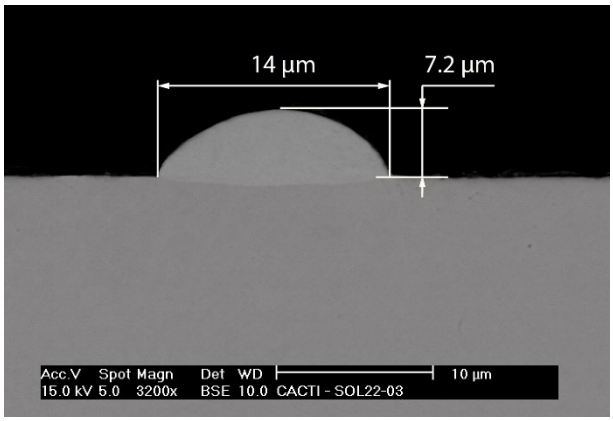

Figure 13**.** Cross-section of a micro-clad produced under optimal processing parameters. (Laser irradiance 38 MW/cm^2, processing speed 18 mm/s, powder mass flow 10 mm/s).

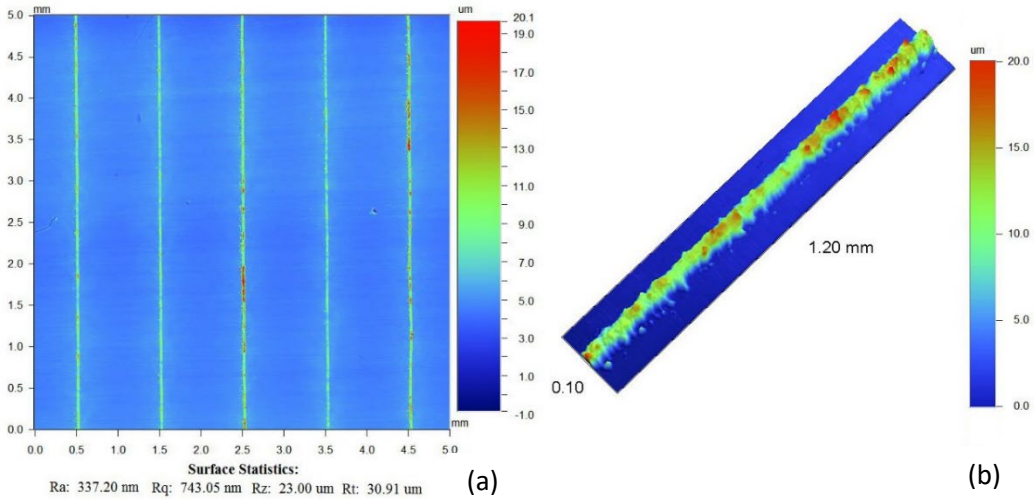

Figure 14. 3D optical suface profilometry of several micro-clad tracks (a). Detail of one of the micro-clad obtained (b).

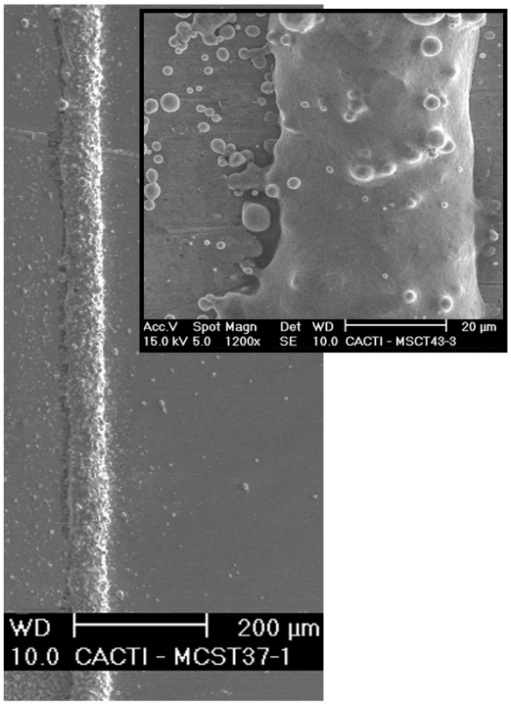

Figure 15. SEM micrograph of the track surface. Inset shows a detail of the surface at higher magnification.

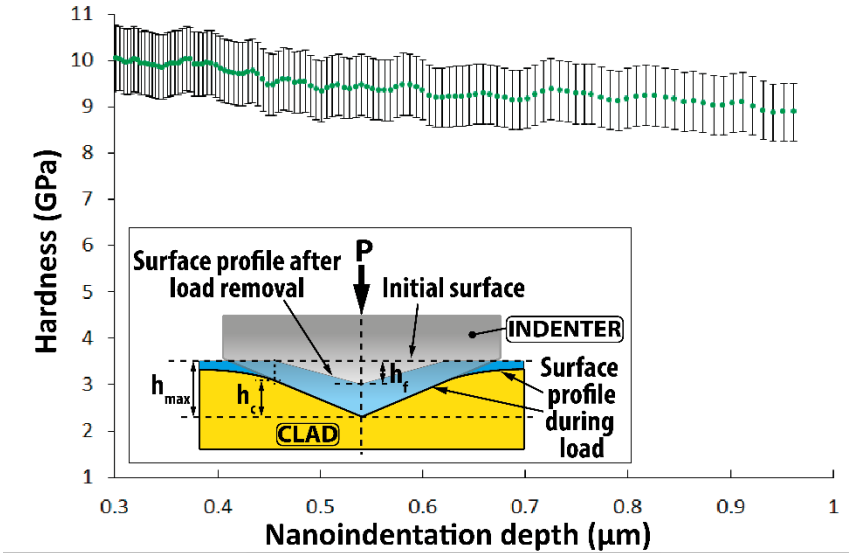

Figure 16. Mean hardness value as function of the displacement of nanoindenter tip into the material.

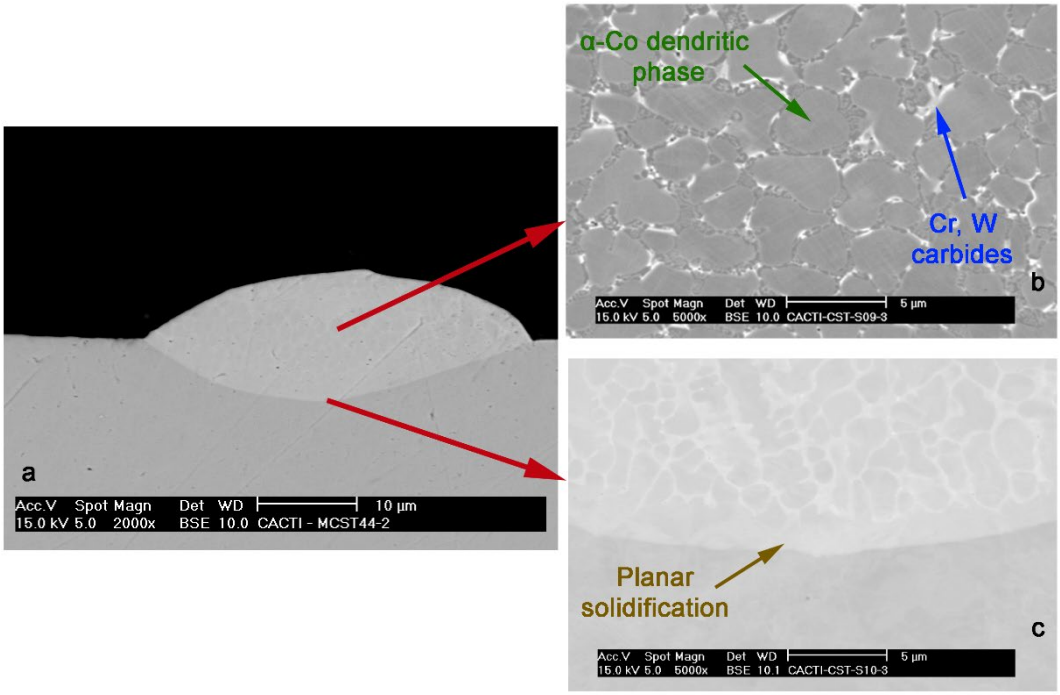

Figure 17. SEM cross section micrograph of micro-meter clad (a). Detail of the microstructure (b), and detail of the interface substrate-clad (c). (Laser irradiance 51 MW/cm^2, processing speed 3.5 mm/s, powder mass flow 10 mg/s).